

# Stability Analysis and Design of Local Control Schemes in Active Distribution Grids

André Eggli, Stavros Karagiannopoulos, Saverio Bolognani, and Gabriela Hug

**Abstract**—The connection of distributed energy resources (DERs) to distribution feeders can significantly increase the operational flexibility of system operators. Local feedback control schemes (such as Volt/VAr droop curves) are a cheap, scalable and communication-free solution to control DERs in active distribution grids. However, these controllers can interfere detrimentally with each other when they act on multiple DERs connected to the same grid. We show that even the standardized curves recommended in the most recent grid codes may exhibit an unstable behavior.

In this paper, we investigate the stability of local incremental DER control laws in three-phase active distribution grids with balanced and unbalanced loading, and we bound the resulting rate of convergence. The use of low-pass filters on the DER set-points allows us to achieve closed-loop stability even for high-gain local control laws that would otherwise destabilize the grid. This feature is particularly relevant in data-driven approaches that yield optimal DER local control schemes, often in the form of steep customized piece-wise linear Volt/VAr curves.

**Index Terms**—active distribution networks, data-driven control design, local Volt/VAr control, stability analysis.

## I. INTRODUCTION

Traditionally, electrical power was generated by large power plants at the transmission voltage level, while the distribution networks (DNs) at medium and low voltage levels were treated as power sinks. Over the last decades, however, a plethora of Distributed Energy Resources (DERs), such as distributed generators and new types of controllable loads have been and are being installed in DNs [1].

One of the most important modern challenges to the Distribution System Operators (DSOs) is to control power flows in order to avoid power quality constraint violations. Most DERs, such as residential photovoltaic (PV) units, can be controlled in order to alleviate these crucial power quality issues and achieve a more efficient grid utilization.

### A. Distributed Power Flow Management via DERs

Based on the available communication and monitoring infrastructure, DER control schemes can be broadly categorized into “centralized”, “distributed” and “local”. In centralized schemes, measurement data from sensors are collected by one central control unit which calculates the optimal set-points to each DER individually, and communicates the command-signals [2], [3].

A. Eggli, S. Karagiannopoulos, and G. Hug are with the Power Systems Laboratory, ETH Zurich, 8092 Zurich, Switzerland.

S. Bolognani is with the Automatic Control Laboratory, ETH Zurich, 8092 Zurich, Switzerland.

Email: {aeggli,bsaverio}@ethz.ch, {karagiannopoulos,hug}@eeh.ee.ethz.ch

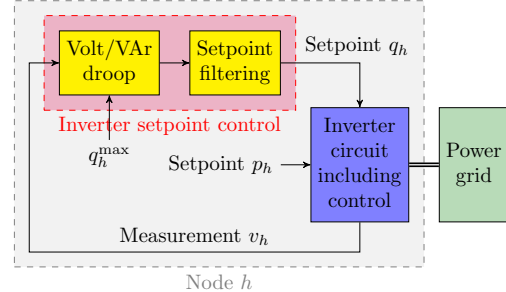


Fig. 1. Schematic representation of the control architecture for the update of DER reactive power setpoints based on local measurements.

Distributed control schemes require limited communication and can achieve near-to-optimal system's performance without any centralized computing unit [4], [5]. Communication links can be employed between critical nodes only, making this approach more affordable compared to centralized schemes. The predominant control architecture, however, prescribes *local control schemes* that do not require any communication, and comprise the most *scalable* and *practical* solution implemented in DNs. Each DER relies on local measurements to adjust its own set-points according to some predetermined rule.

The analysis that we present in this paper applies to local DER control schemes with a completely decentralized architecture. In the presentation of our results, we focus in particular on strategies designed to control reactive power flows and to avoid violations of voltage magnitude constraints. The local Volt/VAr controllers proposed in the literature [2], [6]–[11] differ in terms of the control algorithm and the required local measurements.

In this work we consider the general class of strategies represented in Fig. 1, where the *voltage magnitude measurement* is used as an input to derive the desired set-point for the DER's

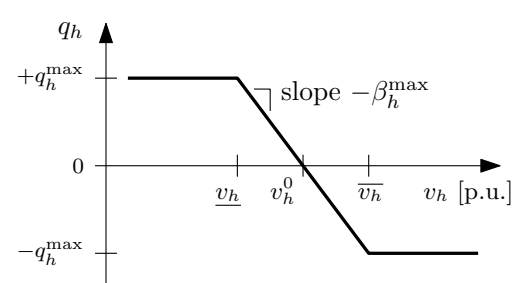


Fig. 2. An example of a Volt/VAr droop curve without low-pass filter and dead-band, compatible with the IEEE 1547 standard [12].

reactive power injection via a static droop function. This set-point may be filtered before being used as a reference for the power inverter controller. One simple example of such a purely local feedback law for reactive power control is reported in Fig. 2.

The fast response of the inverter-based DERs raise new stability concerns and challenges that need to be considered in the planning and operation of active distribution grids [13]. In order to provide an overview and clearly highlight the contributions of our paper, we classify modern dynamic issues into three categories: a) Power circuit control stability and existence of an equilibrium, which is the focus of many works that focus on the converter-level stability exploring very fast phenomena with small time constants; b) Network-wide stability of the setpoint-update strategy, i.e. the stability of the closed-loop behavior that emerges when many inverter-based DERs are simultaneously connected to the grid, which is the focus of this paper; and c) Design of the control laws to regulate the voltage satisfactorily. This final category refers to the design of the individual update strategy for the power set-points of each device, so that the resulting equilibrium satisfies some given specifications.

In practice, most Volt/VAr control schemes (including modern grid codes, e.g. [12], [14], [15]) adopt a one-solution-fits-all approach for the design of these static droop curves, based on standardized voltage deviation bounds and irrespective of the location of each DER or of the specific grid specifications. Alternatively, data-driven approaches have been proposed for the design of the Volt/VAr curves in order to account for several objectives. These methods derive optimized local schemes that emulate the optimal behavior using off-line optimal power flow calculations and machine learning tools [16]–[18].

### B. Motivational Case Study

To further motivate our research and to highlight the importance of the proposed analysis, we briefly investigate stability of the standardized Volt/VAr curve reported in Fig. 2, where we fixed the design parameters according to the recommendations of multiple modern grid codes [12], [14], [15]. According to these standards, high (low) local voltage magnitude will trigger reactive consumption (injection). The absorption (generation) of reactive power mitigates the local overvoltage (undervoltage). However, this feedback scheme can become unstable in some operating regions as can be demonstrated in the following example: Let us consider the benchmark distribution network<sup>1</sup> represented in Fig. 3, featuring four Distributed Generators (DGs) connected to the Cigre benchmark LV test system [19]. We set all active and reactive power loads as well as the active power infeeds from the PVs to a constant value for all 19 nodes. The simulation is initialized by setting the initial DG reactive power injections to some random value which is then adjusted based on the control curve. Consequently, all nodes are treated as PQ nodes in the following power flow computation. As shown in Fig. 4, the reactive power injections do not converge and they engage in a persistent limit cycle. The time interval between update steps

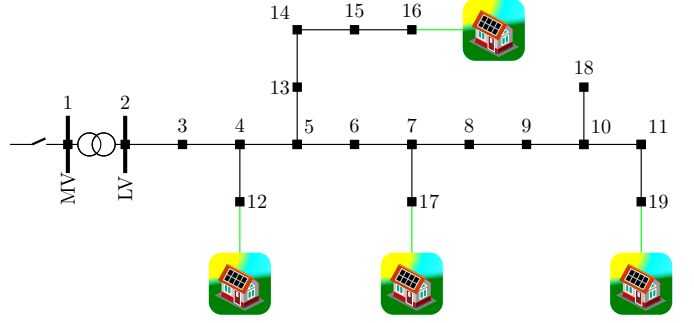


Fig. 3. Modified Cigre LV benchmark grid [19].

is chosen such that all inverter dynamics have decayed between subsequent setpoint updates. The software implementation of this case study is available as a CodeOcean capsule [20].

This simple example motivates our work on the stability of such local Volt/VAr control schemes. It is important to note that both in this example, as well as in the rest of the paper, we assume that DERs periodically adapt their reactive power injection based on their measurements, and  $t$  is the index of such iteration updates. The real absolute time between two iterations does not affect our analysis, as long as this time is longer than the settling time of the power converters and the grid dynamics. In fact, even the actual grid codes [12], [14], [15] do not specify specific values for these iteration updates.

### C. Related work and original contributions

In contrast to [21], we follow a discrete time approach, which, we believe, is a more accurate model of these control schemes. We also allow nonlinearity of the control law when we derive explicit analytic expressions for the system's stability, without the need for numerical simulations and without resorting to small-signal stability analysis tools (e.g., damping ratios) that unrealistically assume linearity of the controllers.

A small-signal analysis around individual equilibria is also proposed in [6], [11]. By providing a global stability certificate, we can instead guarantee that these control strategies do not jeopardize safe grid operation in any operating condition.

The analysis in [10] is restricted to the special case of purely proportional droop curves with saturation, and the authors of [22] assume the same Volt/VAr curve given by the grid standard IEEE 1547.8 [12] for all DERs. Instead, our certificates apply to arbitrary and heterogeneous droop curves and therefore can be systematically incorporated in

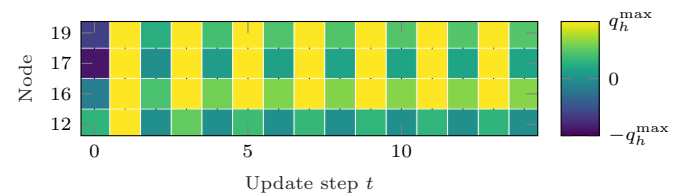


Fig. 4. Oscillatory DER reactive power injections observed in the motivational case study presented in Section I-B.

<sup>1</sup> The details of this benchmark are provided in Section VI.

the automated tuning procedures of the aforementioned data-driven approaches [16]–[18].

Finally, we show how it is possible to allow steeper Volt/VAr curves (and therefore satisfy more stringent specifications) by introducing a first-order filter in the feedback control loop, which was also advocated by [6] (but without a large-signal stability analysis).

The original contributions of this paper are:

- a guarantee of existence and uniqueness of the equilibrium for a wide class of nonlinear droop-like DER control laws in three-phase distribution grids;
- a stability analysis of these control laws based on a discrete-time model of their interaction;
- an analysis of the trade-off between steepness of the droop curves of the local schemes and dynamic closed-loop performance;
- an analytical derivation of the worst case rate of convergence of the local rules;
- a numerical demonstration of the proposed method using a benchmark LV residential grid.

The remainder of this paper is structured as follows: In Section II, we define the underlying regulation problem and introduce an incremental control scheme. In Section III, we provide conditions on the Volt/VAr curves that guarantee the existence of a unique equilibrium. The convergence to this equilibrium is discussed in Section IV, while Section V investigates the convergence speed, resulting in recommendations on control parameter tuning. A case study based on the CIGRE benchmark DN is conducted in Section VI, and conclusions are drawn in Section VII.

## II. DYNAMIC MODEL

Let us consider a grid connected, balanced, symmetric<sup>2</sup> distribution network. For each bus  $h \in \mathcal{V} := \{0, \dots, N\}$  the following rms quantities are defined:  $v_h$  is the voltage magnitude,  $p_h$  the active and  $q_h$  the reactive power injection. All nodes are modelled as constant power buses. Node 0 denotes the point of common coupling (PCC). We assume  $v_0 = 1.0$  p.u. for the PCC, independent of the power flow. Nodes  $h \in \mathcal{N} := \{1, \dots, n\} \subset \mathcal{V}$  are each connected to a DER, which measures the local voltage magnitude  $v_h$  and adjusts its reactive power setpoint according to some local control law. Voltage measurements and reactive power setpoint adjustments occur at discrete time steps  $t = 1, 2, 3, \dots$ . The DERs' reactive power setpoints are held constant between consecutive measurements. Further, we assume that all DERs are synchronized to a common clock signal. Each DER measures the local voltage magnitude at time  $t + 1$  and instantly reacts by updating its reactive power injection setpoint according to an incremental control strategy of the form

$$q_h(t+1) = (1 - \lambda) \cdot q_h(t) + \lambda \cdot f_h(v_h(t+1)), \quad (1)$$

where  $\lambda \in (0, 1]$  can be interpreted as a low pass filter parameter and  $f_h$  is a nonlinear droop curve. Notice that with

<sup>2</sup> Unbalanced, asymmetric three-phase DNs are considered in the Appendix as supplementary material.

TABLE I  
TYPICAL TIME CONSTANTS IN DER CONTROL AND DYNAMIC STABILITY

Phenomena / control loop	Typical time constants
Power line dynamics	< 1 ms
Pulse-Width Modulation	< 1 ms
Harmonics	< 1 ms
Power inverter control	1–10 ms
Power inverter set-points control	> 100 ms

$\lambda = 1$  we recover standard static Volt/VAr droop strategies of the form  $q_h(t+1) = f_h(v_h(t+1))$ .

We define  $v$  (and, similarly,  $q$ ) as the vector containing all voltage magnitudes measured by the DERs. Then, (1) can be written as:

$$q(t+1) = (1 - \lambda) \cdot q(t) + \lambda \cdot f(v(t+1)), \quad (2)$$

with  $[f(v)]_h := f_h(v_h)$ .

We consider a single-phase grid and approximate the influence of reactive power injection on the steady-state voltages (i.e., when grid, load, and inverter dynamics have settled) as

$$v_{ss}(q) \approx Xq + \tilde{v}, \quad (3)$$

where the matrix  $X \in \mathbb{R}^{n \times n}$  is related to the grid's susceptance when linearizing around a flat voltage profile and zero power flows. The matrix  $X$  can be constructed following [22] or [4]. The value of  $\tilde{v}$  is not controllable as it depends on the active power of the loads and DERs, as well as the reactive power of the loads. As proven in [22],  $X$  is real, positive definite and symmetric. In the following, we consider (3) as an equality. The approximation quality of this step is discussed in [22].

**Assumption 1.** *The power system dynamics (grid, load, and inverter dynamics) reach steady state between iterations, i.e.*

$$v(t+1) = v_{ss}(q(t)),$$

where  $v_{ss}$  is the steady state map provided in (3).

This assumption includes two aspects. On the one hand, it implies that the interconnected power converters (and their controllers) can inject the desired reactive-power setpoint  $q$  and operates in that regime in a stable manner. Depending on the specific type of converter and their internal controllers, this may limit the region of feasible reactive power injections that can be safely commanded to the DERs. On the other hand, Assumption 1 implies that the low-level control schemes of the power converters settle to their steady-state before a new reactive-power setpoint is passed to them. This is reasonable in practice, due to the time-scale separation of the power system phenomena [13] and of the different control loops (see Table II).

Under Assumption 1 we can combine (2) and (3), and obtain the closed loop dynamics

$$q(t+1) = \underbrace{(1 - \lambda) \cdot q(t) + \lambda \cdot f(Xq(t) + \tilde{v})}_{:=\Phi(q(t))}. \quad (4)$$

The domain of the map  $\Phi(\cdot) : C \rightarrow C$  is the joint reactive power injection capability of all DGs, i.e.

$$C := [-q_1^{\max}, q_1^{\max}] \times \cdots \times [-q_n^{\max}, q_n^{\max}], \quad (5)$$

where  $[-q_h^{\max}, q_h^{\max}]$  denotes the injection capability of node  $h \in \mathcal{N}$  (Appendix B extends the model to DERs whose reactive power capability depends on their active power injection).

### III. EXISTENCE OF A UNIQUE EQUILIBRIUM

In this section we prove the existence of a unique reactive power injection equilibrium for the map  $\Phi$  defined in (4), provided constant active and reactive load.

We define  $q^*$  as a reactive power injection that satisfies the equilibrium relation

$$\Phi(q^*) = q^*. \quad (6)$$

**Proposition 1.** *The dynamics (4) have a unique equilibrium  $q^*$ , solution of (6), provided that all  $f_h(\cdot)$  are continuous and weakly decreasing. Moreover, such an equilibrium is independent of  $\lambda$ .*

*Proof.* After simple manipulations we can rewrite the equilibrium relation (6) as

$$q^* = f(Xq^* + \tilde{v}), \quad (7)$$

which is independent of  $\lambda$ . By defining  $x := Xq^*$ , equation (7) is equivalent to

$$X^{-1}x - f(x + \tilde{v}) = 0. \quad (8)$$

The inverse of any symmetric, positive definite matrix is symmetric, positive definite as well. Let us further define

$$\Upsilon := X^{-1} - \kappa\mathbb{I}, \quad (9)$$

where  $\kappa > 0$  denotes the smallest eigenvalue of  $X^{-1}$ . The smallest eigenvalue of  $\Upsilon$  is zero, which makes this matrix positive semidefinite.

Inserting (9) into (8) leads to

$$\Upsilon x + \tilde{f}(x) = 0, \quad (10)$$

where we have defined  $\tilde{f}(x) := -f(x + \tilde{v}) + \kappa x$ . Note that  $\tilde{f}(\cdot)$  is a strictly increasing function. As proven in [23], equation (10) has one unique solution  $x^*$ , which corresponds to a unique reactive power equilibrium  $q^* = X^{-1}x$ . ■

We have therefore proved that the steady state voltage magnitudes after convergence are uniquely determined by the Volt/VAr curves  $f(\cdot)$  and by the load/generation profile. A crucial aspect of this result is that this guarantee is provided *a-priori* for any droop curve that satisfies the continuity and monotonicity condition, rather than being an *a posteriori* numerical test on a given curve. This fact implies that the desired voltage quality can be sought for by properly designing the Volt/VAr curves before deployment, and irrespective of the low-pass-filter parameter  $\lambda$ , which remains as an additional degree of freedom in the design stage.

### IV. STABILITY

In this section, we investigate the convergence of the dynamics (4) to the unique equilibrium  $q^*$ . More formally, we aim to provide sufficient conditions for global asymptotic stability of the closed-loop system, defined as follows.

**Definition 1** (Global asymptotic stability). *We assume all active and reactive power injections to be constant in time for all nodes  $h' \in \mathcal{V}$ . Exclusively the reactive power injection of the DGs  $h \in \mathcal{N}$  is updated for each time step according to the control law (4). The closed loop system is denoted as globally asymptotically stable, if  $\lim_{t \rightarrow \infty} q(t) = q^*$ , independently of the initial conditions  $q(0)$ .*

In order to present our stability result, we need to introduce some notation. Let  $\beta_h^{\max}$  denote the Lipschitz constant for every Volt/VAr curve, i.e.,

$$\beta_h^{\max} := -\sup_{v \neq v'} \frac{|f_h(v) - f_h(v')|}{|v - v'|} \quad \forall h \in \mathcal{N}. \quad (11)$$

In practical terms,  $\beta_h^{\max}$  corresponds to the maximum absolute steepness of the droop curve  $f_h(v)$ . Notice that the formal definition in (11) does not require differentiability of the functions  $f_h$  and can be applied, for example, to piecewise linear functions. In that case,  $\beta_h^{\max}$  corresponds to the slope of the steepest segment. Further, let

$$B := \text{diag}(\beta_1^{\max}, \dots, \beta_n^{\max}). \quad (12)$$

We then define the critical value  $\bar{\lambda}$  for the filter parameter  $\lambda$  via the following lemma (whose proof is available in Appendix C).

**Lemma 1.** *For any balanced, symmetric, radial DN there exists a  $\bar{\lambda} > 0$  that satisfies*

$$\|(1 - \bar{\lambda})\mathbb{I} - \bar{\lambda}BX\| = 1. \quad (13)$$

Based on these definitions, we can state the main result, which connects the parameter  $\lambda$  of the filter to the steepness parameter  $B$  in order to guarantee global convergence of the control strategy.

**Proposition 2.** *Let all  $f_h(\cdot)$  be continuous and weakly decreasing. Then for any  $\lambda \in (0, \bar{\lambda})$ , the dynamics (4) are globally asymptotically stable and converge to the unique equilibrium point  $q^*$  derived in Proposition 1.*

The remaining part of this section will be used to provide the proof of Proposition 2. To do so, we need to derive the following intermediate technical result.

**Lemma 2.** *Let  $\lambda > 0$  satisfy*

$$\|(1 - \lambda)\mathbb{I} - \lambda BX\| \leq 1. \quad (14)$$

*Then the mapping  $\Phi(\cdot)$  defined in (4) is non-expansive, i.e.*

$$\|\Phi(q') - \Phi(q)\| \leq \|q - q'\| \quad \forall q, q'.$$

*Proof.* We have

$$\begin{aligned} \|\Phi(q) - \Phi(q')\| &= \|\lambda f(Xq + \tilde{v}) + (1 - \lambda)(q - q') \\ &\quad - \lambda f(Xq' + \tilde{v})\| \\ &= \|-\lambda BX(q - q') + (1 - \lambda)(q - q')\| \\ &= \|(1 - \lambda)\mathbb{I} - \lambda BX\|(q - q'). \end{aligned}$$

Notice that in the second equality we consider, without loss of generality, the case where  $v_h = Xq_h + \tilde{v}$  and  $v'_h = Xq'_h + \tilde{v}$  are both within the steepest region of the control curves  $f_h(\cdot)$ , where the slope is equal to the Lipschitz constant  $-\beta_h^{\max}$ . For this particular case we have

$$f(v) - f(v') = -B(v - v') = -XB(q - q'). \quad (15)$$

Note that this step may be overly conservative. For some grids there exists no practically feasible power flow, where all DGs operate simultaneously at the steepest section of their control curve. However, considering that many optimal power flow solutions will likely tend to operating points close to the over voltage limits, such a scenario is definitely reasonable. Including this worst case in our considerations, may additionally be helpful under extreme operating conditions. Unexpected scenarios such as fault conditions may lead the system into an unusual state, where oscillations are even worse than in normal operation. we can therefore conclude that  $\|\Phi(q) - \Phi(q')\| \leq \|q - q'\|$  if (14) is verified. ■

Thus, we can finally prove our main stability result.

*Proof of Proposition 2.* From (4) we have

$$\begin{aligned} q(t+1) &= (1 - \lambda)q(t) + \lambda f(Xq(t) + \tilde{v}) \\ &= \left(1 - \frac{\lambda}{\bar{\lambda}}\right)q(t) + \lambda f(Xq(t) + \tilde{v}) + \frac{\lambda}{\bar{\lambda}}q(t) - \lambda q(t) \\ &= \left(1 - \frac{\lambda}{\bar{\lambda}}\right)q(t) + \frac{\lambda}{\bar{\lambda}}((1 - \bar{\lambda})q(t) + \bar{\lambda}f(Xq(t) + \tilde{v})), \end{aligned}$$

that is

$$q(t+1) = \left(1 - \frac{\lambda}{\bar{\lambda}}\right)q(t) + \frac{\lambda}{\bar{\lambda}}\bar{\Phi}(q(t)), \quad (16)$$

where

$$\bar{\Phi}(q(t)) := (1 - \bar{\lambda})q(t) + \bar{\lambda}f(Xq(t) + \tilde{v}).$$

Notice that  $\bar{\lambda}$  exists via Lemma 1 and  $\bar{\Phi}(q(t))$  is a non-expansive map via Lemma 2, as  $\bar{\lambda}$  clearly satisfies (14). Moreover,  $\bar{\Phi}(q(t))$  is a continuous map (therefore, compact) from the bounded, closed, convex set  $C$  defined in (5) to itself. Finally, observe that  $\frac{\lambda}{\bar{\lambda}} \in (0, 1)$ .

We can then apply [24, Theorem 3.2] and conclude that the trajectories  $q(t)$  in (16) converge to a fixed point of  $\bar{\Phi}(q(t))$ . According to Proposition 1, the only fixed point of  $\bar{\Phi}(q(t))$  is  $q^*$ . Therefore,  $q(t)$  must converge to  $q^*$ . ■

## V. RATE OF CONVERGENCE

In the previous sections, we examined the impact of the feedback curves  $f$  on the system's steady state, which is not affected by the filter parameter  $\lambda$ . However,  $\lambda$  and  $f$  jointly affect the stability of the system, which is ensured by Proposition 2 that prescribes a tuning range for the parameter  $\lambda$  as a function of the Lipschitz constants  $\beta_h^{\max}$ .

In this section, we exploit this tuning freedom in order to optimize the convergence speed of the proposed scheme, and we illustrate a fundamental trade-off between this convergence speed and the steepness of the Volt/VAr curves. A consequence

of this fact is that stability can be guaranteed even for arbitrarily steep droop curves, by sacrificing convergence speed.

We start by defining the contraction rate

$$\mu(q) := \frac{\|v(\Phi(q)) - v(q^*)\|}{\|v(q) - v(q^*)\|}, \quad (17)$$

where  $\Phi(\cdot)$  is defined in the update equation (4) and  $q^*$  is the equilibrium from Proposition 1. The rate  $\mu$  is a function of the filter parameter  $\lambda$ , as well as the current state  $q$ . A uniform upper bound on  $\mu$  (i.e., independent from  $q$ ) is of particular interest for design purposes, as it provides a worst-case guarantee on the dynamic performance of the closed-loop system. We therefore define the *convergence rate*  $R(\lambda)$  as

$$R(\lambda) := \max_q \mu(q). \quad (18)$$

In the following, we study the rate of convergence under two assumptions, which allow to perform a small signal analysis of the rate of convergence under different operating regimes.

**Assumption 2.** All Volt/VAr curves  $f_h(v_h)$  are saturated linear droop curves of the form

$$f_h(v_h) = \text{sat}_{q_h^{\min}}^{q_h^{\max}}(-\beta_h^{\max}(v - v_h^0)). \quad (19)$$

In practical terms, Assumption 2 prescribes a reactive power injection which varies linearly between a lower voltage bound  $v_h$  (at which point the DER injects the maximum reactive power  $q_h^{\max}$ ) and an upper voltage bound  $\bar{v}_h$  (where the DER draws the maximum reactive power), as shown in Figure 2.

**Assumption 3.** The considered DN is radial, balanced and symmetric, and thus the matrix  $X$  has only real eigenvalues.

### A. Convergence rate in unsaturated regime

Let us consider the case where all the DERs do not reach their reactive power injection limit, and therefore operate in the linear part of their Volt/VAr curve. More formally, for both  $q$  and  $q^*$  we have  $v(q) \in [\underline{v} \ \bar{v}]$  and  $v(q^*) \in [\underline{v} \ \bar{v}]$ , where  $\underline{v}$  and  $\bar{v}$  are defined in Assumption 2. We therefore have

$$\begin{aligned} R(\lambda) &= \max_q \frac{\|v(\Phi(q)) - v(q^*)\|}{\|v(q) - v(q^*)\|} = \\ &\stackrel{1}{=} \max_q \frac{\|X(\Phi(q) - q^*)\|}{\|X(q - q^*)\|} = \\ &\stackrel{2}{=} \max_q \frac{\|X(\Phi(q) - \Phi(q^*))\|}{\|X(q - q^*)\|} = \\ &\stackrel{3}{=} \max_q \frac{\|X[(1 - \lambda)\mathbb{I} - \lambda BX](q - q^*)\|}{\|X(q - q^*)\|} = \\ &= \max_q \frac{\|[1 - \lambda]\mathbb{I} - \lambda XB\| X(q - q^*)\|}{\|X(q - q^*)\|} \\ &= \|(1 - \lambda)\mathbb{I} - \lambda XB\|, \end{aligned} \quad (20)$$

where;

in  $\stackrel{1}{=}$  we used the linear grid model (3),

in  $\stackrel{2}{=}$  we used the equilibrium condition  $\Phi(q^*) = q^*$ , and

in  $\stackrel{3}{=}$  we used the fact that all DERs are operating in a point where the slope of  $f_h$  is  $-\beta_h^{\max}$ .

For a balanced, symmetric DN (Assumption 3) we follow the reasoning in the proof of Lemma 1 and arrive at

$$\|(1 - \lambda)\mathbb{I} - \lambda XB\| = \|(1 - \lambda)\mathbb{I} - \lambda\Delta\| \quad (21)$$

where the matrix  $\Delta$  is real diagonal, with all its diagonal entries  $\xi_i \geq 0$ , i.e.,

$$\Delta := \text{diag}(\xi) \quad \text{with } \xi_i \in \text{eig}(TXT), \quad (22)$$

where  $T := B^{1/2}$ . We define  $\bar{\xi}$  and  $\underline{\xi}$  as the upper and lower bound on these eigenvalues

$$\bar{\xi} := \max_i \xi_i, \quad \underline{\xi} := \min_i \xi_i.$$

We can therefore express the rate of convergence as

$$R(\lambda) = \max\{1 - \lambda(1 + \underline{\xi}), |1 - \lambda(1 + \bar{\xi})|\}. \quad (23)$$

Such an expression can be optimized analytically. Let us define  $\lambda^* := \arg \min_{\lambda} R(\lambda)$ . Solving (23) for  $\lambda^*$  leads to

$$\begin{aligned} 1 - \lambda^*(1 + \underline{\xi}) &= -(1 - \lambda^*(1 + \bar{\xi})) \\ \iff \lambda^* &= \frac{2}{2 + \bar{\xi} + \underline{\xi}}. \end{aligned} \quad (24)$$

For this particular choice of  $\lambda$ , we achieve the rate of convergence

$$R(\lambda^*) = \frac{\bar{\xi} - \underline{\xi}}{2 + \bar{\xi} + \underline{\xi}}. \quad (25)$$

### B. Convergence rate in (partially) saturated regime

We now relax the assumption that all DERs are operating in the linear part of their Volt/VAr droop curve. Namely, we assume that a subset of DERs  $\mathcal{M} \subset \mathcal{N}$  operates in a saturated regime, and more precisely any  $h \in \mathcal{M}$  operates in the zero-sloped segment of their Volt/VAr curve:

$$\begin{aligned} f_h(v_h(q)) &= f_h(v_h(q^*)) = q_h^{\min} \\ \text{or } f_h(v_h(q)) &= f_h(v_h(q^*)) = q_h^{\max}. \end{aligned}$$

We use the same notation and symbols as in the last subsection, but adding the dependence on  $\mathcal{M}$  to denote this partially saturated case. We define the diagonal matrix  $B(\mathcal{M})$  whose diagonal elements are

$$[B(\mathcal{M})]_{hh} = \begin{cases} \beta_h^{\max} & h \notin \mathcal{M} \\ 0 & h \in \mathcal{M}. \end{cases}$$

This augmentation affects the entries of  $\Delta$ , since the lowest eigenvalue  $\underline{\xi}'(\mathcal{M})$  of  $B$  in the expression  $T(\mathcal{M})XT(\mathcal{M})$  will be zero. Therefore, we introduce the notation  $\Delta(\mathcal{M})$  according to (22) with corresponding diagonal entries set to zero. Depending on  $\mathcal{M}$ , the largest eigenvalue  $\bar{\xi}'(\mathcal{M}) > 0$  may be smaller than  $\bar{\xi}$  in the linear case. In analogy to (24) we arrive at

$$R_{\mathcal{M}}(\lambda) = \max\{1 - \lambda, |1 - \lambda(1 + \bar{\xi}(\mathcal{M}))|\} \quad (26)$$

which is minimized by

$$\lambda^*(\mathcal{M}) = \frac{2}{2 + \bar{\xi}(\mathcal{M})}, \quad (27)$$

yielding

$$R_{\mathcal{M}}(\lambda^*(\mathcal{M})) = 1 - \lambda^*(\mathcal{M}) = \frac{\bar{\xi}(\mathcal{M})}{2 + \bar{\xi}(\mathcal{M})}. \quad (28)$$

Due to the local nature of the control architecture that we are considering, DERs can not adjust their control parameter  $\lambda$  depending on the set  $\mathcal{M}$  according to (27). The parameter  $\lambda$  needs to be predetermined offline, with careful consideration of possible saturation conditions.

Notice from (27) and (24) (and from the fact that  $\bar{\xi}(\mathcal{M}) \leq \bar{\xi}$ ) that  $\lambda^*(\mathcal{M}) \geq \lambda^*$ . In other words, the optimal value for filter parameter  $\lambda$  is larger (faster filter) in the saturated case. Choosing  $\lambda < \lambda^*$  is therefore not recommended from the performance point of view. In contrast, choosing  $\lambda > \lambda^*$  might be beneficial in certain cases. A numerical case study will examine particularly this matter in Section VI-C.

### C. Convergence rate in fully saturated regime

We finally consider the case where all DERs are saturated. The analysis in this case can be simply obtained by following the reasoning in the last subsection for  $\mathcal{M} = \mathcal{N}$ . We obtain  $B(\mathcal{N}) = 0$  and  $\bar{\xi}(\mathcal{N}) = \underline{\xi}(\mathcal{N}) = 0$ . The rate of convergence in this case is only determined by the filter parameter  $\lambda$ , namely

$$R_{\mathcal{N}}(\lambda) = 1 - \lambda. \quad (29)$$

The rate of convergence is therefore maximized by choosing a large  $\lambda$  (fast filter), as long as the condition  $\lambda < \bar{\lambda}$  is satisfied to guarantee stability in the other working regimes.

## VI. CASE STUDY

In this section, we demonstrate the theoretical findings with a case study, using the Cigre LV benchmark grid already shown in Fig. 3. All physical grid parameters such as line lengths and cable types are taken from [19]. The load and PV panels are distributed to the three phases unevenly, resulting in unbalanced conditions. The total load, taken from [19] is shared 25%-60%-15% among the three phases. The installed PV capacity, is set to  $S_{PV}$  rated = 100% of the total maximum load of the entire feeder to the PV nodes = [12, 16, 17, 19], and is shared 25%-25%-50% among the three phases.

### A. Stability of generalized Volt/VAr curves

Following the methodology of [18], we constructed optimized Volt/VAr curves by fitting optimal setpoints derived from off-line simulations. The resulting curves are sketched in Fig. 5 (for phase C).

Recall from Proposition 2 that we need to choose  $\lambda < \bar{\lambda}$  in order to obtain stable closed-loop dynamics. The value of  $\bar{\lambda}$  can be easily calculated numerically from (13). In order to assess the tightness of this stability condition, we consider a nominal case in which all active and reactive power injections and withdrawals are set to zero, except for the reactive power injection at the DGs. As  $f_h(1) = 0 \quad \forall h \in \mathcal{N}$  in the curves we have constructed,  $q^* = 0$  is an equilibrium (and the only one, according to Proposition 1). We initialize  $q(0)$  to a non-zero vector. The convergence of the closed-loop system to this

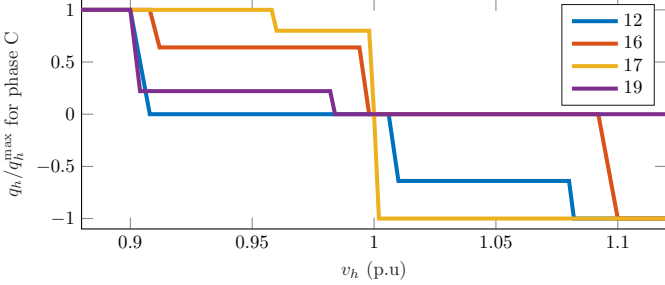


Fig. 5. Exemplary Volt/VAr curves for the different DGs, designed according to the procedure in [18].

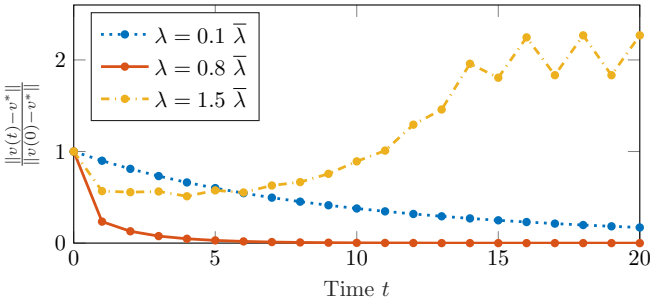


Fig. 6. Convergence analysis for different values of the low-pass filter parameter  $\lambda$ .

equilibrium can be assessed in Fig. 6, that reports the voltage trajectories for different values of  $\lambda$ . The figure shows that  $\lambda = 1.5 \bar{\lambda}$  does not converge to the equilibrium, confirming that the sufficient conditions in Proposition 2 are not too conservative. The reactive power injections  $q(t)$  for this unstable case are shown in Figure 7.

#### B. Rate of convergence in unsaturated regime

In Section V-A we quantified the worst-case rate of convergence when all DGs are operating in the linear region of their Volt/VAr curves. We validate this assessment via a simulation in which the reactive power injection is initialized in the linear region, and the system remains in the linear region for all  $t \geq 0$ . We set  $\lambda = 0.5 \bar{\lambda}$  to guarantee convergence. Figure 8 shows the distance of voltages from the equilibrium

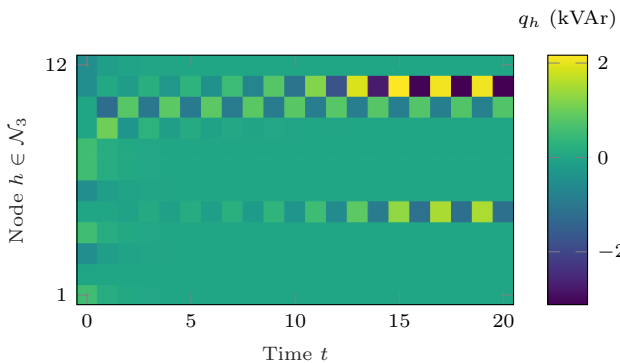


Fig. 7. DER reactive power injections  $q_h(t)$  for  $\lambda = 1.5 \bar{\lambda}$

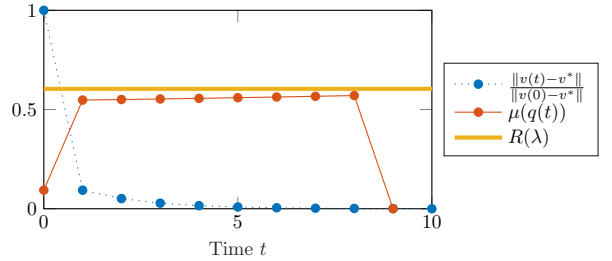


Fig. 8. Contraction rate  $\mu$  over time, together with the worst-case convergence rate  $R(\lambda)$ .

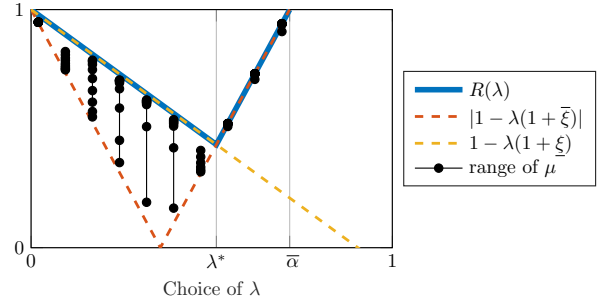


Fig. 9. Contraction rates for different choices of  $\lambda$ , compared to  $R(\lambda)$ .

over time, together with the contraction rate  $\mu$  defined in (17) and its worst-case upper bound  $R(\lambda)$  (computed as in (20), using the extension to three-phase systems reported in Appendix A). We observe that the voltages converge quickly to the equilibrium. Despite being the result of a worst-case analysis,  $R(\lambda)$  provides an accurate upper bound on  $\mu$  at all times.

In Figure 9 the same simulation is repeated for ten different values of  $\lambda$ . For each simulation, we report the contraction rates  $\mu(q(t))$ . The rate  $R(\lambda)$  from (23) bounds all the ten sequences of  $\mu(q(t))$  from above, as expected.

#### C. Convergence rate in (partially) saturated regime

In Section V-B we investigated the closed-loop rate of convergence when a subset  $\mathcal{M} \subset \mathcal{N}$  of DERs operates in the saturated regime. The considered grid contains four DGs,  $\mathcal{N} = \{12, 16, 17, 19\}$ , resulting in  $2^4 = 16$  possibilities to choose the subset  $\mathcal{M}_i$  (see Table II). The case number  $i = 1$  corresponds to *no saturated DGs*. Figure 10 shows the rate  $R_{\mathcal{M}_i}(\lambda)$  according to (26) for every case number  $i$ . The numerical results confirm the intuition developed in Section V-B: choosing  $\lambda < \lambda^*$  yields worse performance than  $\lambda^*$ , in all circumstances. However, choosing  $\lambda > \lambda^*$  is beneficial for complete saturation and for some partially saturated cases. Nevertheless, it yields worse performance in other cases, and notably in the linear regime. This is also true, if we select the largest possible value  $\lambda = \bar{\lambda}$ . This numerical experiment confirms that, without knowing which DGs are saturated, the choice  $\lambda = \lambda^*$  provides the best worst-case dynamic performance of the closed-loop system.

TABLE II  
ALL POSSIBLE SETS OF SATURATION  $\mathcal{M}_i$

$\mathcal{M}_1 := \{$
$\mathcal{M}_2 := \{ 12$
$\mathcal{M}_3 := \{ 16$
$\mathcal{M}_4 := \{ 17$
$\mathcal{M}_5 := \{ 19$
$\mathcal{M}_6 := \{ 12, 16$
$\mathcal{M}_7 := \{ 12, 17$
$\mathcal{M}_8 := \{ 12, 19$
$\mathcal{M}_9 := \{ 16, 17$
$\mathcal{M}_{10} := \{ 16, 19$
$\mathcal{M}_{11} := \{ 17, 19$
$\mathcal{M}_{12} := \{ 16, 17, 19$
$\mathcal{M}_{13} := \{ 12, 17, 19$
$\mathcal{M}_{14} := \{ 12, 16, 19$
$\mathcal{M}_{15} := \{ 12, 16, 17$
$\mathcal{M}_{16} := \{ 12, 16, 17, 19\}$

#### D. Effect of steep Volt/VAr curves on the rate of convergence

Here, we investigate the relation between the slopes of the Volt/VAr curves on the achievable convergence speed, and therefore the resulting tradeoff between high-gain steady state specifications and dynamic performance. Let us assume that all Volt/VAr curves are of the form (19) with equal slopes  $\beta_h^{\max} = \beta \forall h \in \mathcal{N}$ . With increasing values of  $\beta$ , a smaller value of  $\lambda \in (0, \bar{\lambda})$  has to be chosen in order to ensure stability (as seen in Figure 11, where  $\bar{\lambda}$  is plotted together with the optimal  $\lambda^*$ ). Figure 11 also reports the rate of convergence in the linear regime and in the fully saturated case, when the filter parameter  $\lambda$  is optimally tuned, as prescribed in Section V. The result from this case study substantiates the general intuition: the higher the Lipschitz constants (steepness) of the Volt/VAr curves, the smaller  $\lambda$  has to be chosen in order to guarantee stability, which then worsens the rate of convergence  $R$  in both the saturated and non-saturated case.

## VII. CONCLUSIONS

In this paper, we investigated the dynamic behavior of local control schemes for power distribution grids, focusing on Volt/VAr regulation strategies (such as the one recommended in the IEEE 1574 standard). We demonstrated that an oscillatory behavior can be easily observed in the closed loop dynamics. We proposed an incremental implementation of these Volt/VAr schemes, and we derived simple and explicit conditions that guarantee global closed-loop stability. Based on our analysis and guidelines, almost arbitrary Volt/VAr

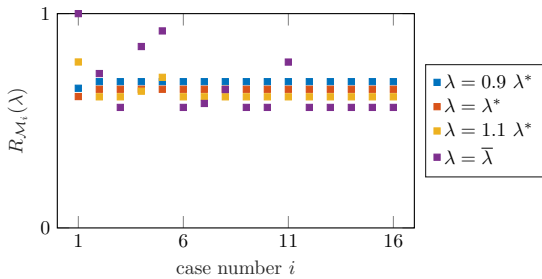


Fig. 10. Convergence rate  $R(\lambda)$  for all subsets  $\mathcal{M}_i$  of saturated DERs.

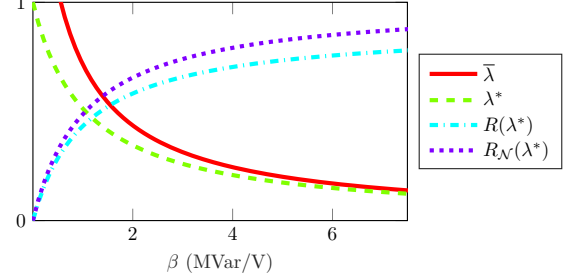


Fig. 11. Influence of the steepness of the Volt/VAr droop curves on the largest stabilizing filter parameter  $\lambda$ , its optimal value, and the resulting rate of convergence.

curves can be employed, once the control is properly tuned. This enables the recent data-driven control schemes to design optimized local scheme for each DG.

We investigated the network-level rate of convergence to the equilibrium and illustrated a fundamental trade-off between the steepness of the Volt/VAr curves and convergence speed. Finally, we provide recommendations for a robust optimization of the dynamic performance.

The results from this paper can be applied in streamlined control parameter tuning in the design stage of localised reactive power injection schemes and mitigate the need for tedious numerical stability considerations.

## APPENDIX A EXTENSION TO THREE PHASE SYSTEMS

The previous sections assumed balanced and symmetric DNs, which enabled us to substitute three phase circuits by a single phase representation. However, practical DNs can be heavily unbalanced, especially if DGs are connected to single phases only. Further, the mutual coupling between the three phases of a line can be asymmetric. We can account for unbalanced asymmetric three phase systems by the following augmentation:

- The set containing all nodes  $\mathcal{V}_3$  is tripled in size compared to  $\mathcal{V} = \{1, \dots, N\}$ . Every phase is now considered a separate bus.
- Consequentially, there will be a separate local Volt/VAr curve for every microgenerator phase. Note that the set of microgenerators  $\mathcal{N}_3$  does not necessarily triple in size, as some PV-inverters may be single phase.

This augmentation allows us to redefine  $X$  according to (3).

### A. Computation of $X$

We follow the steps in [25]: for every line between two nodes  $h$  and  $k \in \mathcal{V}$ , we define a complex valued  $3 \times 3$  admittance matrix  $y_{hk} = (z_{hk})^{-1}$ . The  $3N \times 3N$  nodal admittance matrix  $Y$  is defined as

$$Y_{hk} = \begin{cases} \sum_{l \neq h} y_{hl} & \text{if } k = h \\ -y_{hk} & \text{otherwise} \end{cases} \quad (30)$$

Because we assumed complete absence of shunt elements, it must hold that  $Y\mathbb{1} = 0$ .

Let us define

$$e_0 := \begin{bmatrix} \mathbb{I}_{3 \times 3} \\ 0_{(3N-3) \times 3} \end{bmatrix} \in \mathbb{R}^{3N \times 3}, \quad (31)$$

$$\Theta := \text{diag} \left( \mathbb{1}_{N \times 1} \otimes \begin{bmatrix} 1 \\ e^{-j2\pi/3} \\ e^{j2\pi/3} \end{bmatrix} \right), \quad (32)$$

$$D := \begin{bmatrix} \Theta^{-1} Y \Theta & e_0 \\ e_0^\top & 0_{3 \times 3} \end{bmatrix}^{-1}. \quad (33)$$

We select the top left block of size  $3N \times 3N$  from  $D$  and get  $Z \in \mathbb{R}^{3N \times 3N}$

$$Z := 3 \cdot \begin{bmatrix} \mathbb{I}_{3N \times 3N} & 0_{3N \times 3} \end{bmatrix} \cdot D \cdot \begin{bmatrix} \mathbb{I}_{3N \times 3N} \\ 0_{3 \times 3N} \end{bmatrix}. \quad (34)$$

The matrix  $Z$  represents the first order approximation of the power flow

$$v_{\text{full}} = \Re(Z) \cdot p_{\text{full}} + \Im(Z) \cdot q_{\text{full}}, \quad (35)$$

where the subscript  $\cdot_{\text{full}}$  denotes all nodes in  $\mathcal{V}_3$ . Since we are only interested in the microgenerator nodes  $\mathcal{N}_3$ , we obtain  $X$  by selecting the corresponding entries from  $\Im(Z)$ .

### B. Generalisation of previous results to three phase systems

If  $X$  is positive definite, the proofs of Proposition 1 and Proposition 2 still hold. Note that for the three phase case the eigenvalues of  $X$  and  $B^{1/2}XB^{1/2}$  can become complex. Therefore, (14) has no simple analytic solution and must be checked numerically by sweeping through  $\lambda$ .

## APPENDIX B

### COUPLED PQ INVERTER CAPABILITY CURVE

So far, we considered the reactive power injection limit to be independent of the active power production  $p_h(t)$ . In reference [17], such inverters are referred to as *type 2 inverters* (see Figure 12). This section focuses on *type 1 inverters*, where the reactive power limit depends linearly on active power. Let the set  $\mathcal{W} \subseteq \mathcal{N}$  denote all type 1 inverters. For every node  $h \in \mathcal{W}$  we augment its volt-var curve

$$f'_h(v_h, p_h) = \begin{cases} q_h^{\max} \cdot \frac{p_h(t)}{p_h^{\max}} & , f_h(v_h) > q_h^{\max} \cdot \frac{p_h(t)}{p_h^{\max}} \\ f_h(v_h) & , |f_h(v_h)| < q_h^{\max} \cdot \frac{p_h(t)}{p_h^{\max}} \\ -q_h^{\max} \cdot \frac{p_h(t)}{p_h^{\max}} & , f_h(v_h) < -q_h^{\max} \cdot \frac{p_h(t)}{p_h^{\max}} \end{cases} \quad (36)$$

where  $f_h(\cdot)$  is the original volt-var curve as introduced in Section II, following the definition of  $\beta_h^{\max}$  from (11) and using the non-augmented Volt/VAr curves. While this simplification may be conservative for some operating regions, for simultaneous peak active power output,  $p_h(t) = p_h^{\max}$ , it represents exactly the case considered. As a side effect, the matrices  $B$  and  $X$  are not affected by the augmentation and the stability considerations stated in Section IV are still valid.

The augmented Volt/VAr curves (36) do not violate any of the conditions in Proposition 1. There still exists a unique equilibrium injection  $q^*$ , although clearly a different one.

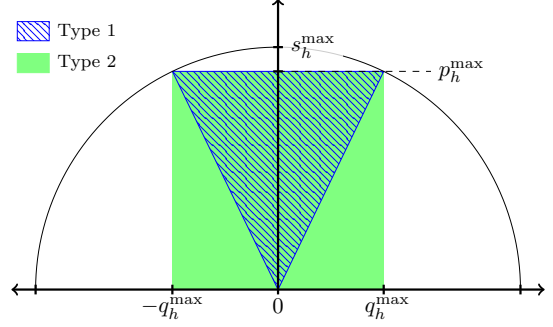


Fig. 12. Inverter PQ-capability curves [17] modified

## APPENDIX C PROOF OF LEMMA 1

Note that  $\beta_h^{\max} \geq 0 \quad \forall h \in \mathcal{N}$  and therefore  $B$  is positive semi-definite. By applying a change of coordinates (via the transformation matrix  $T := B^{1/2}$ ), condition (13) can be rewritten as

$$\|(1 - \bar{\lambda})\mathbb{I} - \bar{\lambda}TXT\| = 1. \quad (37)$$

For a balanced, symmetric, radial DN we know from Section II that the matrix  $X$  is real, symmetric and positive definite. Hence, the matrix  $TXT$  is real, symmetric and positive semi-definite.

According to [26, Theorem 8.32] and [26, Remark after Theorem 8.35], there exists an invertible  $P$  such that  $\Delta = P^{-1}TXTP$  where the matrix  $\Delta$  is real diagonal with all entries  $\xi_i \geq 0 \quad \forall \xi_i \in \text{eig}(TXT)$ , i.e.,

$$\Delta := \text{diag}(\xi_1, \dots, \xi_n).$$

We can therefore rewrite (37) as

$$\|(1 - \bar{\lambda})\mathbb{I} - \bar{\lambda}\Delta\| = 1.$$

The matrix  $(1 - \bar{\lambda})\mathbb{I} - \bar{\lambda}\Delta$  is diagonal, the eigenvalues being the diagonal entries. Its norm consequentially corresponds to the largest diagonal element (in absolute value), i.e.,  $\max_i |1 - \bar{\lambda} - \bar{\lambda}\xi_i|$ . We therefore have  $\|(1 - \bar{\lambda})\mathbb{I} - \bar{\lambda}\Delta\| = 1$  if

$$\bar{\lambda} = \frac{2}{1 + \max\{\xi_i\}} > 0.$$

## REFERENCES

- [1] H. Farhangi, "The path of the smart grid," *IEEE Power Energy Mag.*, vol. 8, no. 1, pp. 18–28, Dec. 2009.
- [2] P. N. Vovos, A. E. Kiprakis, A. R. Wallace, and G. P. Harrison, "Centralized and Distributed Voltage Control: Impact on Distributed Generation Penetration," *IEEE Trans. Power Syst.*, vol. 22, no. 1, pp. 476–483, Feb. 2007.
- [3] S. Karagiannopoulos, P. Aristidou, A. Ulbig, S. Koch, and G. Hug, "Optimal planning of distribution grids considering active power curtailment and reactive power control," *IEEE PES General Meeting*, Jul. 2016.
- [4] S. Bolognani and S. Zampieri, "A Distributed Control Strategy for Reactive Power Compensation in Smart Microgrids," *IEEE Trans. Autom. Control*, vol. 58, no. 11, pp. 2818–2833, Nov. 2013.
- [5] S. Bolognani, R. Carli, G. Cavraro, and S. Zampieri, "On the need for communication for voltage regulation of power distribution grids," *IEEE Trans. Control Netw. Syst.*, vol. 6, no. 3, pp. 1111–1123, Sep. 2019.
- [6] P. Jahangiri and D. C. Aliprantis, "Distributed Volt/VAr Control by PV Inverters," *IEEE Trans. Power Syst.*, vol. 28, no. 3, pp. 3429–3439, Aug. 2013.

- [7] F. Olivier, P. Aristidou, D. Ernst, and T. Van Cutsem, "Active Management of Low-Voltage Networks for Mitigating Overvoltages Due to Photovoltaic Units," *IEEE Trans. Smart Grid*, vol. 7, no. 2, pp. 926–936, Mar. 2016.
- [8] J. W. Simpson-Porco, F. Dörfler, and F. Bullo, "Voltage stabilization in microgrids via quadratic droop control," *52nd IEEE Conf. Decision and Control*, pp. 7582–7589, Dec. 2013.
- [9] N. Li, G. Qu, and M. Dahleh, "Real-time decentralized voltage control in distribution networks," in *52nd Allerton Conf.*, Sep. 2014.
- [10] K. Baker, A. Bernstein, E. Dall'Anese, and C. Zhao, "Network-cognizant voltage droop control for distribution grids," *IEEE Trans. Power Syst.*, vol. 33, no. 2, pp. 2098–2108, 2018.
- [11] A. Singhal, V. Ajjarapu, J. Fuller, and J. Hansen, "Real-time local volt/var control under external disturbances with high pv penetration," *IEEE Trans. Smart Grid*, vol. 10, no. 4, pp. 3849–3859, 2019.
- [12] IEEE 1547-2018, "Standard for interconnection and interoperability of distributed energy resources with associated electric power systems interfaces," Standard, 2018.
- [13] N. Hatziargyriou, J. Milanović, C. Rahmann, V. Ajjarapu, C. Cañizares, I. Erlich, D. Hill, I. Hiskens, I. Kamwa, B. Pal *et al.*, "Stability definitions and characterization of dynamic behavior in systems with high penetration of power electronic interfaced technologies," 2020.
- [14] "VDE-AR-N 4105: generators connected to the LV distribution network - technical requirements for the connection to and parallel operation with low-voltage distribution networks," VDE, Tech. Rep., 2018.
- [15] "Commission regulation (EU) 2016/631 of 14 april 2016 establishing a network code on requirements for grid connection of generators," *OJ*, vol. L112, pp. 1–68, 2016.
- [16] S. Karagiannopoulos, R. Dobbe, P. Aristidou, D. Callaway, and G. Hug, "Data-driven control design schemes in active distribution grids: Capabilities and challenges," in *IEEE PowerTech*, Jun. 2019.
- [17] S. Karagiannopoulos, P. Aristidou, and G. Hug, "Hybrid approach for planning and operating active distribution grids," *IET Generation, Transmission & Distribution*, vol. 11, no. 3, pp. 685–695, Feb. 2017.
- [18] ——, "Data-driven Local Control Design for Active Distribution Grids using off-line Optimal Power Flow and Machine Learning Techniques," *IEEE Trans. Smart Grid*, vol. 10, no. 6, pp. 6461–6471, Nov. 2019.
- [19] K. Strunz, E. Abbasi, C. Abbey, C. Andrieu, F. Gao, T. Gaunt, A. Gole, N. Hatziargyriou, and R. Iravani, "Benchmark Systems for Network Integration of Renewable and Distributed Energy Resources," *CIGRE, Task Force C6.04*, no. 273, pp. 4–6, 4 2014.
- [20] A. Eggli, S. Karagiannopoulos and S. Bolognani, "Stability Analysis and Design of Local Control Schemes in Active Distribution Grids [Source Code]," <https://doi.org/10.24433/CO.2842084.v1>, 2020.
- [21] F. Andrén, B. Bletterie, S. Kadam, P. Kotsampopoulos, and C. Bucher, "On the Stability of Local Voltage Control in Distribution Networks With a High Penetration of Inverter-Based Generation," *IEEE Trans. Ind. Electron.*, vol. 62, no. 4, pp. 2519–2529, Apr. 2015.
- [22] L. C. M. Farivar and S. Low, "Equilibrium and dynamics of local voltage control in distribution systems," in *52nd IEEE Conf. Decision and Control*, 4 2013, pp. 4329–4334.
- [23] I. W. Sandberg and A. N. Willson, "Some theorems on properties of DC equations of nonlinear networks," *The Bell System Technical Journal*, vol. 48, no. 1, pp. 1–34, 1969.
- [24] V. Berinde, *Iterative Approximation of Fixed Points*, 2nd ed. Springer Berlin Heidelberg, 2007.
- [25] S. Bolognani and F. Dörfler, "Fast power system analysis via implicit linearization of the power flow manifold," *53rd Allerton Conf.*, pp. 402–409, Sep. 2015.
- [26] P. J. Olver and C. Shakiban, *Applied Linear Algebra*, 2nd ed. Springer, Cham, 2018.



Power Economy.

**André Egger** was born in Schaffhausen, Switzerland. He received his M.Sc. degree in Electrical Engineering and Information Technology from the Swiss Federal Institute of Technology (ETH Zurich). During his studies, he focused on control engineering aspects related to energy systems and power grids. In 2019, he completed his master thesis in the field of high voltage DC circuit breaking at ETH's High Voltage Lab. Since then, he is working as research associate at Lucerne University of Applied Sciences and Arts at the Competence Centre for



**Stavros Karagiannopoulos** (S'15-M'19) received a Diploma in Electrical and Computer Engineering from the Aristotle University of Thessaloniki, Greece, in 2010, and a M.Sc. degree in Energy Science and Technology from the Swiss Federal Institute of Technology (ETH), Zurich, Switzerland, in 2013. After his M.Sc., he worked at ABB Corporate Research Center in Switzerland until 2015. In 2019 he received the Ph.D. degree from the Swiss Federal Institute of Technology (ETH). Since August 2019, he has been working as a postdoctoral researcher with Power Systems Laboratory at ETH Zurich, and since 2020 also with the Laboratory for Information and Decision Systems at Massachusetts Institute of Technology (MIT). His main research focuses on data-driven and optimization-based methods for active distribution grids.



**Saverio Bolognani** received the B.S. degree in Information Engineering, the M.S. degree in Automation Engineering, and the Ph.D. degree in Information Engineering from the University of Padova, Italy, in 2005, 2007, and 2011, respectively. In 2006-2007, he was a visiting graduate student at the University of California at San Diego. In 2013-2014 he was a Postdoctoral Associate at the Laboratory for Information and Decision Systems of the Massachusetts Institute of Technology in Cambridge (MA). He is currently a Senior Researcher at the Automatic Control Laboratory at ETH Zurich, Switzerland. His research interests include the application of networked control system theory to power systems, distributed control and optimization, and cyber-physical systems.



**Gabriela Hug** (S'05-M'08-SM'14) was born in Baden, Switzerland. She received the M.Sc. degree in electrical engineering in 2004 and the Ph.D. degree in 2008, both from the Swiss Federal Institute of Technology, Zurich, Switzerland. After the Ph.D. degree, she worked with the Special Studies Group of Hydro One, Toronto, ON, Canada, and from 2009 to 2015, she was an Assistant Professor with Carnegie Mellon University, Pittsburgh, PA, USA. She is currently a Professor with the Power Systems Laboratory, ETH Zurich, Zurich, Switzerland. Her research is dedicated to control and optimization of electric power systems.